



LAWRENCE
LIVERMORE
NATIONAL
LABORATORY

Atomistic modeling toward high-efficiency carbon capture: a brief survey with a few illustrative examples

A. Maiti

September 5, 2013

International Journal of Quantum Chemistry

Disclaimer

This document was prepared as an account of work sponsored by an agency of the United States government. Neither the United States government nor Lawrence Livermore National Security, LLC, nor any of their employees makes any warranty, expressed or implied, or assumes any legal liability or responsibility for the accuracy, completeness, or usefulness of any information, apparatus, product, or process disclosed, or represents that its use would not infringe privately owned rights. Reference herein to any specific commercial product, process, or service by trade name, trademark, manufacturer, or otherwise does not necessarily constitute or imply its endorsement, recommendation, or favoring by the United States government or Lawrence Livermore National Security, LLC. The views and opinions of authors expressed herein do not necessarily state or reflect those of the United States government or Lawrence Livermore National Security, LLC, and shall not be used for advertising or product endorsement purposes.

Atomistic modeling toward high-efficiency carbon capture: a brief survey with a few illustrative examples

Amitesh Maiti*

Physical and Life Sciences Division, Lawrence Livermore National Laboratory, Livermore, CA 94550

Abstract

With the negative environmental implications of the anthropogenic emission of greenhouse gases like CO₂ having been scientifically established, emphasis is being placed on a concerted global effort to prevent such gases from reaching the atmosphere. Especially important are capture efforts at large point emission sources like fossil fuel power generation, natural gas processing, and various industrial plants. Given the importance and scale of such activities, it is a significant priority to optimize the capture process in terms of speed, energy requirements, and cost efficiency. For CO₂ capture in particular multiple systems are being pursued both with near-term retrofitting and medium- to long-term designs in mind, including: (1) liquid solvents like amines, carbonates, and ionic liquids; (2) microporous sorbents like zeolites, activated carbon, and metal-organic frameworks; (3) solid sorbents like metal-oxides and ionic clays; and (4) polymeric and inorganic membrane separators. Each system is unique in its molecular-level guest-host interactions, chemistry, heats of adsorption/desorption, and equilibrium thermodynamic and transport properties as a function of loading, temperature and pressure. This opens up exciting opportunities for molecular modeling in the design and optimization of materials systems. Here we offer a brief survey of molecular modeling applications in the field of carbon capture, with a few illustrative examples from our own work.

* E-mail: amaiti@llnl.gov

1. Introduction

From numerous scientific studies and measurements it is now well-established that the amount of CO₂ in the atmosphere have been increasing steadily over the last 150 years – from a steady-state level of 280 ppm just before the industrial revolution in the middle of the 19th century to a current level of just over 400 ppm. Much of this increase in CO₂ concentration has happened in the last 50 years (see Fig. 1), with a clearly increasing trend in the foreseeable future. The historically high levels of CO₂ in the atmosphere have been attributed primarily to anthropogenic emissions, caused by the burning of fossil fuels (coal, oil, petroleum, natural gas) for the purpose of electrical power generation, heavy industries, transportation, etc., as well as other eco-interfering activities, e.g., over-farming, deforestation, and so on. One of the biggest impacts of the elevated CO₂ levels have been a correlated increasing trend in the average surface temperature of the earth, as evident in Fig. 1. Thus, in spite of multi-year-long fluctuations in temperature, with periods as long as a decade or more, the temperature shows a clear increasing trend, from roughly 56.6 F in 1850 to about 58.1 F in 2010. The strong correlation between the levels of CO₂ and time-averaged surface temperature have been attributed to the greenhouse effect in which increased levels of CO₂ (and a few other gases like CH₄, N₂O, chlorofluorocarbons or CFCs) trap some of the heat radiated by the earth's surface thereby leading to an overall rise in the average temperature. The situation is exacerbated by a steadily increasing world population with an enhanced desire for a technology-rich lifestyle, which continues to place even higher demands on energy production. With the realization that clean energy alternatives will take decades to develop, and we have to depend on traditional fossil fuel sources in the immediate future, it has become a high priority to produce energy while simultaneously limiting the atmospheric emission of CO₂ and other greenhouse gases.

Limiting CO₂ emission is a complex task that can be roughly divided into two major sub-tasks: (1) capturing the CO₂ from the output stream; (2) post-processing of the captured CO₂. The post-processing typically involves pressurization of the captured CO₂ into a densified stream followed by long-time sequestration in underground geological reserves, injection into oilfields for enhanced oil recovery, or utilization in various industries including food and beverage, chemical, agricultural, and biological industries. However, most of the cost-intensive and chemically challenging problems are involved in the first step, i.e., CO₂ capture, and that is what we concern ourselves here.

2. Multiple capture strategies, relative costs

From a cost and technological feasibility point of view, most capture strategies have justifiably focused on large point sources like coal plants, heavy industries, natural gas processing plants, and so on. Although on the surface it might appear as the same CO₂ being emitted by various industries, the capture strategy and materials choice depends strongly on the way in which the CO₂ is emitted. For instance, even for an electricity-generating fossil-fuel plant there are several CO₂ capture technology options available, and the proper choice depends on the temperature, pressure, concentration of CO₂ in the output, and the nature of the other gases that it needs to be separated from. The three most commonly discussed strategies in the order of increasing ease in carbon capture are [1]: (1) post-combustion, the most standard technology that involves the burning of the fossil fuel in air thereby leading to dilute CO₂ in the flue gas. The carbon capture in this technology is expensive because of the need to separate a dilute CO₂ stream (typically 10-14% by volume) from N₂; (2) pre-combustion, in which the coal/biomass is gasified in controlled (sub-stoichiometric) amount of oxygen to produce CO and H₂ (syngas), which is further subjected to a water gas shift reaction to produce CO₂ and H₂ (clean fuel). Separating a denser stream of CO₂ from H₂ is a chemically easier process and less expensive than in post-combustion; (3) oxy-combustion, which involves burning fossil fuels in pure oxygen as opposed to air, thereby producing a relatively pure stream of CO₂ with an easy capture step. In order to select an appropriate technology one needs not only to look at the relative ease of carbon capture for each choice, but also the overall cost of implementing such technology, which may be a complex analysis in itself. For instance, although the oxy-combustion process obviates the need for expensive carbon capture step, the very process of creating pure O₂ for combustion involves an expensive O₂/N₂ separation step. On the other hand, post-combustion capture may incur an expensive carbon capture step, but it involves the cheapest and the most tried method of energy production from fossil fuel. In addition, it is relatively straightforward to retrofit a post-combustion power plant with a carbon capture capability. One also has the option of reducing CO₂ emission by using higher efficiency fuel, e.g., high-grade coal (anthracite or bituminous), or high-quality natural gas. The above discussion shows the necessity of a carbon capture scientist to be cognizant of various technology options available, the relative economics involved [2, 3], and device a capture strategy accordingly.

3. Commonly explored capture methods and materials systems

In order to remove the CO₂ from an output stream mixture, one would typically employ a materials system that has more affinity to the CO₂ relative to the other gases in the stream. This affinity could be realized in the form of absorption (binding within the bulk of an absorbing medium), adsorption (binding at the external or internal surface of the capture medium), or selective permeability. Absorption and adsorption can involve either chemical or physical binding of the captured CO₂. Some of the general features of each of these capture strategies, along with the common materials systems employed are listed below:

- **Chemical binding**
 - Common media: Liquid solvent absorbents (Amines, carbonates)
 - Strong binding, Post-combustion
 - Desorption (regeneration) at ~ 100-120 °C
 - Has been commercially used to capture and re-utilize CO₂ for enhanced-oil-recovery
 - Water heating penalty involved, solvent regeneration expensive

- **Physical binding**
 - Common media: Nanoporous solid adsorbents (zeolites, MOFs, ZIFs, layered clays); Physical solvents (ionic liquids, selexol, etc.)
 - Generally weaker binding, but surface can be coated or functionalized to enhance binding
 - Water (and therefore large heating penalty) avoided
 - Large number of possible variations (zeolites, MOFs, ionic liquids)
 - better suited for pre-combustion capture

- **Membrane separations (permeability)**
 - Common media: Polymeric membranes (glassy, rubbery); Ceramic membranes (metal-oxide, zeolite)
 - Polymer membranes have better processability, ceramic membranes perform better at higher T
 - Usually driven by pressure difference
 - Better suited for pre-combustion capture

There are a few additional strategies, *e.g.*, cryogenic separation (selective frosting) that can be cost-effective

in separating CO₂ from streams with already-high CO₂ concentrations and in producing pure streams of liquid CO₂.

4. Opportunities for molecular modeling

Given the many different strategies and materials systems, carbon capture is a fertile ground for applying diverse modeling techniques to the discovery, design, and optimization of capture materials and process parameters. In particular, modeling and simulations at the atomistic level can be used to explore and analyze many material-dependent structural, energetic, thermo-physical, chemical, kinetic, and transport properties associated with the capture process. Listed below are some of the specific areas where modeling can play an important role:

- **Understanding and controlling basic chemistry and interactions:**
 - Heat of absorption/adsorption, Heat of desorption (regeneration)
 - Solubility of various gases (CO₂, N₂, O₂, etc.) as a function of T and P
 - Relative concentrations (phase diagram) of all molecular and ionic species in reactants, products, and intermediates

- **Tailoring physical/ thermodynamic/ transport properties of capture medium**
 - Specific heat, Viscosity, Permeability for specific structures
 - Variations of the above with changing functional groups

- **Speeding up of uptake/ stripping processes**
 - Understanding capture kinetics
 - Rational design of catalysts

- **Novel capture systems/ modes**
 - Atmospheric carbon capture?
 - Biomimetic methods?

- **More efficient, less GHG-emitting fuels**
 - Molecular models of high-grade coal

5. Examples of molecular modeling in carbon capture

The diverse nature of the problems listed above mandates employing diverse modeling techniques. For instance, to understand and optimize chemisorption processes a Quantum mechanical (QM) approach is necessary, while physical binding processes are best addressed by classical molecular dynamics (MD) or Monte Carlo (MC) simulations. In order to estimate physicochemical properties like density, viscosity, or transport and study their variations as a function of different molecular structures, one may utilize correlation approaches based on quantitative structure-property relationship (QSPR) or quantitative structure-activity relationship (QSAR). To study the solubility of gases or liquids in various solvents one may use a QM-based approach with an implicit solvent representation, and to study phase diagrams of molecular and ionic species during a chemical reaction a semi-empirical thermodynamic approach like the UNIFAC, NRTL, or variants thereof may be more appropriate. Below, we illustrate the use of different modeling techniques through a few application examples.

5.1. Heats of CO₂ absorption in primary and tertiary amines

Among all post-combustion methods of carbon capture the most economically viable method at this time appears to be amine scrubbing, i.e., dissolution into aqueous solutions of amines [1, 4]. The most widely studied amines in this regard are primary amines like monoethanolamine (MEA) and sterically hindered tertiary amines like N-methyl-diethanolamine (MDEA), as represented by the general chemical formula $R-NR'-R''$. For MEA: $R = C_2H_4OH$ (ethanol), $R' = R'' = H$; while for MDEA: $R = R'' = C_2H_4OH$, $R' = CH_3$. There is an extensive knowledge of the physical and chemical properties of CO₂ in such amines, such as solubility and vapor-liquid equilibrium [5-14], heats of absorption [14-18], and activation energies [19-21]. Generating such knowledge database requires significant experimental measurements and/or parameter development. Exploration of new and multi-component systems or catalysts could greatly benefit from atomistic modeling that could be used to optimize and screen properties as a function of altering various functional groups. There are ample opportunities in this area given that there have only been limited attempts to apply first-principles QM techniques to the study of CO₂/amine chemistry

[22-25] in a solvent environment.

For most amines, including MEA and MDEA solutions chemical dissolution (chemisorption) is much more favorable than physisorption (except for high CO₂ loading levels), and physically absorbed CO₂ almost spontaneously goes into one of two ionic forms, i.e., carbamate (R-NR'-COO⁻) or bicarbonate (HCO₃⁻). One also needs to note that carbamates cannot form in tertiary amines (because both hydrogens of the NH₂ group are substituted by functional groups), while for primary (as well as secondary) amines both ionic forms are a possibility. Thus, as far as MEA and MDEA are concerned one would need to consider the following reactions:



Since all reactions above occur in a solvent environment, any atomistic calculations need to take the solvents into account, either explicitly or implicitly. Since explicit solvent representation makes a QM calculation computationally prohibitive, we chose an implicit scheme based on the COSMO-RS methodology [26, 27, 28], in which one represents both the solute and solvent molecules by the histogram of their surface screening charges called the σ -profile. All interactions, including coulombic, van der Waals, and hydrogen bond interactions are then defined in terms of these σ -profiles. One can use this formalism to compute the partition function, the Gibbs free energy, and many other important thermodynamic quantities. For instance, COSMO-RS has recently been used to compute the pKa values of a number of aqueous amines [29]. To obtain the σ -profiles of various species in reactions (R1-R3) we employed the all-electron DFT code Turbomole [30, 31], with the Becke-Perdew exchange-correlation functional [32-34] and TZVP basis set [35, 36]. The heat of reaction for each of the three reactions was obtained by taking the difference of the free energies of the reactants from that of the products (for CO₂ we use the internal energy of an isolated molecule in the gas phase), with the assumption that this difference is dominated by the internal energy changes and that the entropic contribution is small. The energy difference of a CO₂ molecule in the gas phase and that in a physisorbed state in the solution phase depends on the amine and its concentration, and was found to be ~ 8 kJ/mol or less.

Given that one is primarily interested in concentrated amine solutions because of higher CO₂ capture capacity per unit solution volume, we considered the most concentrated solutions of MEA and MDEA explored in the literature, i.e., 30 wt% MEA (aq) and 45 wt% MDEA (aq). Table 1 displays the computed ΔH for these amine solutions at 25 °C for the three chemisorption reactions R1-R3 at various levels of CO₂ loading, defined as the molar ratio of CO₂ to the amine. From these results one notes that: (i) All reactions (R1-R3) are highly exothermic (i.e., $\Delta H < 0$), implying a high degree of CO₂ absorption in either carbamate or bicarbonate (or both) forms at room temperature; (ii) ΔH has a small dependence on the CO₂ loading level: for MEA they become slightly more negative (i.e. absorption is even more favored) as a function of increasing CO₂ loading, while for MDEA it is the opposite. This leads to an increasing differential heat of absorption ΔH_{diff} for MEA (for small CO₂ loading) and decreasing ΔH_{diff} for MDEA with increase in CO₂ loading; (iii) Carbamate formation in MEA (R1) is energetically more favorable than bicarbonate formation (R2). However, the magnitude of ΔH in R₂ is *more than half* of that in R₁. Since carbamate formation involves 2 amine molecules while bicarbonate involves only 1, the above fact implies that up to about 0.5 CO₂ loading carbamate should be the primary species, while above 0.5 loading the bicarbonate fraction should increase. Such a picture is indeed consistent with ion speciation data, both from experimental measurements [11, 12] and from detailed e-NRTL models [8, 9, 10]; (iv) The heat of absorption is significantly lower for the tertiary amine, which is consistent with its higher proton affinity as compared to primary amines [37].

For a proper quantitative interpretation of the results in Table 1, one not only needs to be aware of the accuracy of the COSMO-RS, but also the physical assumptions behind such calculations. For instance, the calculations in Table 1 were performed assuming completely dissociated ions. This assumption is certainly good at low loading levels, while at loading > 0.5 one should expect a significant degree of ion-pair association. For more accurate modeling, one should also include the possibilities of the formation of other species, e.g., oxazolidones [11] and other byproducts [12], which could potentially affect the ΔH values. To ascertain the accuracy of the ΔH values for lower loadings, we computed the differential heats of absorption ΔH_{diff} defined by the equations:

$$\Delta H_{diff} = \frac{\partial}{\partial n_{CO_2}} \left[\Delta H^{(1)} n_{COO^-} + \Delta H^{(2)} n_{HCO_3^-} \right] \quad \text{for MEA, and}$$

$$\Delta H_{diff} = \frac{\partial}{\partial n_{CO_2}} \left[\Delta H^{(3)} n_{HCO_3^-} \right] \quad \text{for MDEA,}$$

where n_{CO_2} , n_{COO^-} , and $n_{HCO_3^-}$ are the number of dissolved CO_2 molecules, carbamate ions, and bicarbonate ions respectively, and $\Delta H^{(i)}$ represent the (composition-dependent) absorption heats of the corresponding reaction $[Ri]$ ($i = 1, 2, 3$), as given in Table 1.

Fig. 2 plots the differential heat of absorption in the two amine solutions as a function of CO_2 loading up to 0.7, in which we used the experimental ion speciation values [11, 12] for the MEA and MDEA solutions of our interest. The MEA results are in reasonably good agreement with experimental trends [14-18], including a sharp drop at around CO_2 loading of 0.5, which signifies the onset of HCO_3^- formation. On the other hand, although the result for MDEA is good at the infinite dilution limit [15], it remains much flatter with increasing CO_2 loading. Older experimental data shows much more pronounced decrease with increasing CO_2 loading [14], while more recent data [16, 17] have a flatter behavior, although still decreasing more rapidly than the trend in Fig. 2. Such disagreement is probably due to the fact that at higher loadings there is a significant degree of ion-pair association, which can affect activity coefficients and free energies. These small disagreements notwithstanding, the overall results can still be considered encouraging given the simplicity of the calculations without any parameter adjustment. It shows that such a methodology could be employed to optimize the ΔH of CO_2 absorption and regeneration, a quantity of fundamental importance in CO_2 capture economics.

5.2. Changes in density and specific volume upon CO_2 absorption

Atomistic modeling, especially classical MD can be very useful in computing bulk physical properties, e.g., any density and volume changes associated with CO_2 chemisorption. There are several interesting questions in this regard, e.g., the dependence of volume change on the anion type (bicarbonate vs. carbamate), the CO_2 loading levels, and the degree of ion association. Experimental results [38-41] indicate that the prior to any CO_2 absorption, the density of a 45 wt% aqueous MDEA solution ($\sim 1.04 \text{ g/cm}^3$) [38, 39] is higher than that of a 30 wt% aqueous MEA solution ($\sim 1.01 \text{ g/cm}^3$) [39, 40], not a surprising fact given that pure MDEA has a higher density [41] than pure MEA [40]. Both amines display negative excess volumes (i.e. density enhancements) upon mixing with water, and in both solutions the density increases with increasing CO_2 levels. However, the rate of density increase with CO_2 loading is higher in MEA than in the MDEA solution, and for 0.5 CO_2 loading, the density of the MEA solution is actually slightly higher than that of the MDEA solution [39, 40]. Analysis of the change in density of the two

amine solutions as a function of CO₂ loading reveals that the increase in volume per absorbed CO₂ is much lower in MEA (~ 3.5 Å³/ CO₂) as compared to MDEA (~ 9.4 Å³/ CO₂), corresponding to a faster rate of density increase in the MEA solution [42].

To understand the above difference in volume changes in the two solutions at the atomistic level we performed classical molecular dynamics (MD) simulations on pure amines and their aqueous solutions using the Materials Studio software [43]. The inter-atomic interactions were described by a general-purpose state-of-the-art class II forcefield COMPASS [44], widely validated for condensed-phase systems like organic liquids. Simulations were performed on pure amine systems, i.e., water, MEA, and MDEA, as well as two solution systems of our interest, i.e., a 30 wt% MEA solution and a 45 wt% MDEA solution for two CO₂ loading levels, i.e., 0 and 0.5. Cubic periodic supercells were used to represent all systems, employing 400 and 100 molecules respectively for pure water and pure amine systems, while both the aqueous amine solutions were represented by 50 amine and 400 water molecules (corresponding to 11.1% mole fraction amine) with 25 CO₂ molecules added to represent 0.5 CO₂ loading level. We carried out 100 ps simulations in the *NPT* ensemble under ambient conditions employing the Anderson thermostat and barostat [45], which preserves the cell shape during volume change, while long-range coulomb interactions were treated with the Ewald summation technique [46, 47].

The MD simulations yield a number of interesting results, including: (1) accurate densities for the amine solutions without prior to any CO₂ loading; (2) a significant density enhancement for chemisorbed CO₂ as compared to physisorbed CO₂; and (3) a clearly increasing rate of density enhancement for MEA (carbamates) as compared to MDEA (HCO₃⁻) as a function of CO₂ loading. However, at 0.5 CO₂ loading the computed densities in both amines are overestimated by about 3% as compared to experimental values [39, 40]. The higher density increase in MEA is somewhat counterintuitive because the smaller bicarbonate ions in MDEA are expected to have a tighter solvation shell [39]. This argument might be applicable in systems in which the ions are isolated from each other, i.e., for very low CO₂ loading levels. However, at 0.5 CO₂ loading levels the MD trajectories show a high degree of association, i.e., pairing of anions and cations. From an analysis of the Voronoi volumes of various ions and molecules in the MD trajectories we conclude that although the local density of the HCO₃⁻ ions is on an average higher than that of the MEA-carbamate ions, there is a Voronoi volume *decrease* of ~ 4-6 Å³ upon the formation of a carbamate ion (relative to a neutral MEA molecule), while the Voronoi volume of a HCO₃⁻ increases by 3-4 Å³ relative to a neutral

H₂O molecule [42]. This is probably the key reason behind the higher density increase in MEA upon CO₂ chemisorption.

5.3. Alternatives to MEA

In spite of a rich history and knowledge on primary amines, a few successful applications on CO₂ capture have so far been made only at smaller scale pilot projects. Before commercial-scale application at large power plants can become economically viable, some serious challenges need to be addressed, including: (1) CO₂ chemisorption involves a relatively high ΔH and therefore high energy requirements for solvent regeneration; (2) CO₂ stripping typically involves steam, which incurs a significant loss of heat in unnecessary heating of water; (3) amines like MEA is corrosive, thus limiting the amine concentration in the aqueous solution, which limits absorbed density of CO₂; (4) finite volatility of smaller amines, which involves both solvent loss and environmental pollution; and (5) chemical degradation of amines at high operating temperatures. In addition, as mentioned in the previous section, primary and secondary amines absorb CO₂ in the form of carbamates (for CO₂ loading up to 0.5), which involves two amine molecules per absorbed CO₂. A more attractive option would be to form HCO₃⁻ ions, which doubles the CO₂-capture efficiency of the solvent.

Several possible alternatives to MEA have been suggested by various research groups. For instance, sterically hindered amines with bulky side-groups can lower the stability of carbamate ions, thereby leading to the formation of more HCO₃⁻ upon CO₂ absorption. Examples of such amines include 2-amino-2-methyl-1-propanol (AMP) (primary) and 2-piperidinethanol (PE) (secondary). Other, more complex hindered amines have also been commercially explored, such as the proprietary series KS-1, KS-2, KS-3 from Mitsubishi. One could also use tertiary amines like MDEA, where carbamate formation is completely prohibited (see section 5.1). However, the CO₂ absorption and desorption process in such systems is much slower as compared to MEA, and one needs to use catalysts and promoters to improve the rate kinetics. One of the most studied classes of promoters to speed up CO₂ capture by tertiary amines is based on piperazine (PZ), a cyclic amine [4, 48, 49]. However, there are many possible derivatives of PZ that could be systematically studied to optimize this process, and molecular modeling, including correlations based on molecular descriptors could play an important role in screening for efficient and economically viable candidates.

A second class of solvents that has been explored in connection with CO₂ capture is carbonate solutions (K₂CO₃, Na₂CO₃) where CO₂ is absorbed in the form of HCO₃⁻. Compared to amines, such solvents have several advantages, including: (1) inexpensive; (2) stable at high temperatures; (3) already used in the processing of natural gas, syngas, and town gas; (4) can remove both CO₂ and S-containing impurities from the flue gas, etc. Speed of CO₂ absorption-desorption is a major drawback, to overcome which researchers are drawing a cue from nature and trying to design biomimetic catalysts that can speed up the process. For instance, animals use a class of enzymes called carbonic anhydrase to speed up the process of CO₂ conversion to HCO₃⁻ and back. The active site of this enzyme contains a metal center with a Zn²⁺ ion. QM-based atomistic modeling [50] in conjunction with stopped-flow spectrophotometry has recently been used to identify the rate-limiting steps in the CO₂ → HCO₃⁻ → CO₂ conversion process. Such understanding could help in the molecular design of catalysts that can potentially speed up the CO₂ capture kinetics.

The solvents considered so far involve the ones where CO₂ undergoes chemisorption. Such solvents have strong ΔH and are ideal in situations where the CO₂ is in dilute concentration, e.g., post-combustion capture. From an economy as well as speed point of view, one would prefer a medium that would capture the CO₂ physically, i.e., as CO₂ itself without any chemical reactions involved. Two important types of solvents in this regard are glycol-based solvents (that use the so-called Selexol process) and molten salts that are liquids at temperatures of 100 °C or lower, called ionic liquids. Much of the atomistic modeling has been used to screen, model, and analyze the performance of ionic liquids, and we consider one such application below.

5.4. Screening of ionic liquids for CO₂ capture efficiency

Ionic liquids (ILs) [51-54] constitute an alternative solvent system that offers distinct advantages over traditional solvents like MEA, some of which include: (1) high chemical stability; (2) low corrosion; (3) almost zero vapor pressure (*i.e.*, “green”); (4) supportable on membranes [55]; (5) does not involve an aqueous medium (thus avoiding unnecessary heating of water during solvent regeneration) and (6) a huge library of anion and cation choices, which can be potentially optimized for CO₂ solubility and selectivity. In addition, CO₂ dissolves physically in most ILs,

thus significantly lowering the energy requirements for CO₂ release (and solvent regeneration). Over the last few years several ILs have been experimentally demonstrated [56-63] to be efficient solvents for CO₂. Given a huge library of ILs with potentially high CO₂ solubility, and the fact that each experiment costs time and money, theoretical modeling is an attractive tool in a systematic screening of ILs for efficiency in dissolving CO₂. Standard atomic level simulations, e.g., molecular dynamics, or binding-energy calculations can provide useful insights into the interactions of CO₂ with the cation and the anion [64-66]. However, accurate solubility computation in such complex fluids faces many challenges, including accurate force field development, clever Monte Carlo moves [67], and very long simulation times for good statistical averaging.

For fast computation of solubility with reliable accuracy, it is highly desirable to adopt a general-purpose thermodynamic approach that computes the chemical potential of a solute (CO₂ in this case) in any solvent at arbitrary dilution. A widely used program in this regard is COSMO-RS [26-28], as introduced in section 5.1. COSMO-RS uses the surface-charge histogram or the σ -profile to compute a number of thermodynamic quantities, including the pseudo-chemical potential (μ^*) (i.e., the Gibb's free energy per molecule without the ideal mixing entropy contribution). If the pseudo-chemical potential of a solute molecule in a solution containing x mole-fraction of the solute is $\mu_{solution}^*(x, T)$, and that in the solute's own liquid environment is $\mu_{self}^*(T)$, then under dilute conditions, the solubility (in mole-fraction) is given by the expression [28]:

$$x = \exp\{[\mu_{self}^*(T) - \mu_{solution}^*(x, T)]/k_B T\},$$

where T is the absolute temperature and k_B the Boltzmann constant, respectively.

The COSMO-RS program was originally developed with the aim of modeling condensed phases, primarily liquid, with solubility and liquid-liquid phase equilibrium being one of its primary application domains. For a solid dissolving into a liquid solvent one needs to include an additional contribution due to the heat of fusion, while to represent a nonconventional liquid like an IL, one creates a 50-50 random mixture of the individual σ -profiles of the cationic and anionic constituents of the IL [28]. We have recently used this formalism to screen efficient solvents for a hard-to-dissolve energetic material [68]. From extensive tests on the aqueous solubility of a large dataset of drug molecules and organic solutes it appears that COSMO-RS incurs an average error of the order of 0.3-0.5 log units [69]. Based on this, an accuracy of the computed solubility to within a factor of 2-3 can be considered reasonable.

At the same time the COSMO-RS errors are not random, but are rather systematic within classes of solvents. Therefore, one can still expect to obtain useful trends from such calculations. There have been several recent reports on COSMO-RS computation of CO₂ solubility in different ILs [70-74] with the aim of uncovering trends that can serve as a guide to solvent optimization.

One challenge for the present application is that the solute species (CO₂) is dissolving not from the solid or liquid, but from the gas phase. Although, there is a standard prescription of computing gas solubility with COSMO-RS that involves the experimental vapor pressure, this can lead to a severe overestimation of CO₂ solubility at a given pressure and temperature as compared to experimental results [75]. Instead, we have shown that the following equation works better with consistent accuracy:

$$P = \frac{P^0}{\phi(P, T)} x \exp\left\{\frac{\mu_{solution}^*(x, T) - \mu_{ig}^*(T)}{k_B T}\right\}$$

where x is the molar solubility at pressure P and temperature T , $\phi(P, T)$ is the fugacity coefficient of the dissolving gas, and μ_{ig}^* is the dilute-limit pseudo-chemical potential of the ideal dissolving gas defined at a low reference pressure of $P^0 = 1$ bar. To use the above equation successfully, the following strategy was adopted:

- 1) The quantity $\mu_{solution}^*(x, T)$ was computed by COSMO-RS using the standard settings as describe in section 5.1.
- 2) The fugacity coefficient ϕ was computed using the standard formula:

$$\ln(\phi) = (k_B T)^{-1} \int_0^P (V - k_B T / P) dP,$$

using the Soave-Redlich-Kwong (SRK) [76, 77] equation of state (EOS) for CO₂. The fugacity coefficient ϕ monotonically decreases as a function of increasing P and decreasing T . At T around T_c , the SRK EOS is known to become less accurate for P greater than P_c [77]. Thus, our analysis was confined to P not much higher than $P_c = 73.7$ bar (for CO₂).

- 3) Finally, a proper computation of $\mu_{ig}^*(T)$ within the COSMO-RS framework would involve a complete analysis of the differences between partition function of a free molecule and a molecule in the condensed phase, including rotational, translational, vibrational, and zero-point contributions. Fortunately, in practice, a simple empirical free-energy correction term appears sufficient for the subcritical region $T < 0.7 T_c$ [28]. However, for

the near-critical and supercritical region of our interest, corrections to the COSMOtherm-computed μ_{ig}^* became necessary. From extensive numerical experiments, we found that the following simple 2-parameter formula works well in the 20-100 °C temperature range:

$$\mu_{ig}^*(T) = \mu_{ig}^*(T_c) + \alpha(T - T_c).$$

In our previous work [78] we tested the above formalism on a limited dataset and recommended values of $\mu_{ig}(T_c) = -4.43$ kcal/mol and $\alpha = -0.02$ kcal/mol/K. The emphasis in that work was placed on establishing the validity of the above computational scheme and looking for consistency in solubility trends rather than the optimization of the accuracy of the predicted solubility. When a larger dataset of CO₂ solubility measurements is included, the computed solubility using the above parameter values displays a significant bias, as recently pointed out [79]. As a remedy, these authors suggested an additional pressure-dependent parameter in the fit for $\mu_{ig}^*(T)$.

We show below that it is unnecessary to introduce any additional parameters, either involving pressure-dependence or non-linear dependence on temperature. Rather, just a simple optimization of the parameter values to $\mu_{ig}(T_c) = -4.10$ kcal/mol and $\alpha = -0.019$ kcal/mol/K solves the problem, as shown in Fig. 3 (left). Note that the experimental data points correspond to several temperatures, varying between 20 °C and 100 °C, and the accuracy of the results does not deteriorate at elevated temperatures. The mean deviation in predicted fugacity as compared to the experimental values (for a given solubility level of CO₂) is ~ 5.5 bar. Above pressures of 15 bar the solubility, on an average, is predicted to within an accuracy of 20%, much more accurate than the average error of 0.3-0.5 log units that COSMO-RS is generally known to incur [69].

Although the above parameters work well at higher pressures, a careful examination of lower pressure data ($P < 20$ bar) reveals a bias in that the computed fugacity consistently overestimates the experimental value, sometimes by as much as 50% or higher. If one wishes to focus on the low pressure region and Henry's constant only (e.g., post-combustion capture), one needs to slightly modify the first parameter, i.e., $\mu_{ig}(T_c) = -3.97$ kcal/mol, while the temperature-dependence parameter α remains unchanged (see Fig. 3 (right)).

Using the new optimized parameters we screened for the IL solvents with the best solubility of CO₂ in the range of pressures 30-50 bar and at $T = 40$ °C. Fig. 4 displays the computed results at $P = 50$ bar as a function of twelve

different cations for a fixed anion [Tf₂N], one of the most commonly studied anions with a high mole-fraction solubility for CO₂. Fig. 4 plots the CO₂ solubility both in mole-fraction (*x*) and in a more practical molality scale, defined by the number of moles of CO₂ dissolved per kg of the solvent:

$$\text{molality (mol/kg)} = \frac{x}{(1-x)M_w},$$

where *M_w* is the molecular weight of a solvent ion-pair in kg/mol. The molality scale emphasizes the amount (i.e. mass) of solvent required to dissolve a given amount of CO₂. The most notable results from Fig. 4 are:

- the mole-fraction solubility increases as a function of the size of the functional group on the cations, as evident from the orderings: [emim] < [bmim] < [hmim] < [omim]; [tbp] < [ttp]; [tma] < [tea] < [tba]; and [hmg] < [ppg];
- for the ions chosen in this group, the molal solubility follows the same order as the mole-fraction solubility in spite of the increasing molecular weight of the larger functional groups. The only exception is [ttp] < [tbp], and is clearly a result of [ttp] possessing a much higher molecular weight than [tbp] (see Table 2). The case of [ttp] having lower molal solubility of CO₂ than [tbp] implies that the molal solubility within a cationic class attains a maximum value for ions of masses somewhere in the range 200-400 g/mol depending on the class;
- by comparing different classes with similar functional groups we can draw the conclusion that the molal solubility increases in the order imidazolium < phosphonium ~ ammonium < guanidinium.

To see which cation-anion combination (within our limited set) could lead to an IL with the maximum molal solubility of CO₂, we computed the CO₂ solubility in six different anions ([BF₄], [PF₆], [Tf₂N], [NO₃], [TfO], and [FEP]) (see Table 3) and three different cations ([omim], [tba], and [ppg]). The three cations chosen are the most efficient (within our data set) solvent representatives of the three classes imidazolium, ammonium, and guanidinium respectively (the results for phosphonium are very similar to ammonium and are not reported separately). Fig. 5 displays the results at *T* = 40 °C and *P* = 30 bar. The most notable results are:

- for the imidazolium class [FEP] leads to the highest mole-fraction solubility, in agreement with a previous publication [80] while Tf₂N is a close second. However, within the ammonium and the guanidinium classes, [FEP] is not as efficient. [Tf₂N] appears to possess the highest or near-highest mole-fraction across all cationic classes, which perhaps justifies the reason for it being one of the most studied IL anions;

- for both ammonium and guanidinium classes the molal solubility increases in the order [FEP] < [Tf₂N] < [PF₆] < [TfO] < [BF₄] < [NO₃]. This order nearly holds for the Imidazolium class as well, with the molal solubility of the middle four groups being close to each other. In particular, note that [FEP] is the least efficient and [NO₃] the most efficient for all cations in terms of molal solubility;
- overall, the efficiency order in terms of molal solubility appears to be imidazolium < ammonium < guanidinium, as also seen in Fig. 3. In particular, [PPG][NO₃] possess the highest molal solubility of CO₂, roughly 2.6 times (i.e. 160 % higher) as compared to [omim][NO₃], the highest value for the most commonly studied imidazolium class. Interestingly, for the imidazolium class the [NO₃] group does not stand out in its mole-fraction solubility of CO₂. That could be the reason why much attention was not paid to it in our previous study [78] where [PPG][BF₄] was assigned the most efficient solvent within the data set.

One should note that the molal solubility in [omim][NO₃] is high simply because of the small size of the [NO₃] anion. However, for the ammonium and guanidinium groups even the mole-fraction solubility is the highest or near-highest in presence of the [NO₃] anion. This, in combination with its small size makes the molal solubility in [NO₃] much higher. This is especially true for [PPG], where the mass of the cation is also smaller compared to [omim] or [TBA]. It should be mentioned that the above search was by no means exhaustive, and leaves much room for systematic improvements. In order to perform a search on millions of potential candidates one would need to set up an automated search procedure, as has recently been done on screening for zeolites [81, 82].

It should also be recognized that the viability of any theoretically predicted new IL candidate should be tested for its physicochemical properties, e.g., melting point, density, viscosity, specific heat, etc. Since synthesis and characterization on any new IL is expensive, developing correlations of these quantities based on simple to calculate properties from a molecular model could be very useful. Some progress toward that front has been made by Krossing and co-workers [83, 84], where interesting correlations between the above IL properties and their molar volumes (V_m) have been observed. Quantities like V_m can be reliably computed using COSMO-RS just from the knowledge of the molecular structures of the component ions of the IL.

Since physisorption involves weak binding, ILs as such are more appropriate for CO₂ capture in a pre-combustion process. In order to extend their utility to post-combustion capture, where the concentration of CO₂ is low, the binding could be enhanced by functionalizing ILs with amines. The first such attempt was made by tethering an

amine group (NH₂) to a cation [85]. These cations bind CO₂ in the form of carbamates, and therefore two molecules are required to capture one CO₂. Recently, it has been shown that by tethering an amine group to a specific anion one can absorb two CO₂ molecules in one functionalized anion. The absorption occurs sequentially – through the formation of a first carbamic acid group (as opposed to a carbamate), followed by a ring closure, and then the formation of a second carbamic acid group. The stability of these species and the feasibility of such chemistry have been confirmed by both DFT-based calculations and IR characterization [86, 87].

5.5. Modeling membranes for CO₂ capture

Although most small to medium scale demonstration of carbon capture have so far been carried out in liquid medium, primarily amines, significant research efforts have been and are being carried out in using membranes for separating and isolating CO₂. Two most important concepts related to any membrane separation are Permeability and Selectivity. Permeability (P) is defined by the equation:

$$P = \frac{QL}{A\Delta p}$$

where Q is the amount of gas flow per unit time, L the thickness of the skin layer, A the cross-sectional area, and Δp the pressure difference between the two sides of the skin. Selectivity is defined as the ratio of the permeability of various gases (or fluids) through the membrane. Thus, the selectivity of a membrane toward gas 1 as compared to gas 2 is defined as $\alpha_{1/2} = P_1/P_2$.

There are several possible mechanisms of gas permeation through a membrane, including Knudson diffusion, surface diffusion, capillary condensation, molecular sieving, and solution-diffusion. Of these, the last two mechanisms are the two most actively investigated. Materials used for molecular sieving primarily include zeolites, metal-organic frameworks (MOFs), and zeolitic imidazolate frameworks (ZIFs). Given that the atomic structures of such materials are known, there have been extensive atomistic modeling efforts toward designing and optimizing such materials for CO₂ capture [88-98], both in membrane and bulk configurations. Most of these simulations have involved classical MD or MC, the success of which depends critically on the accuracy with which the employed force field describes the interaction between the adsorbed guest molecules and the framework of the capture

material, as well as assumptions about the framework response (e.g., structural rigidity). In spite of challenges in designing force fields with accurate non-bond parameters (Coulomb, van der Waals) that are transferable across a wide-variety of frameworks, there have been a number of encouraging successes, including: (1) a systematic investigation of the effects of metal-oxide, organic linker, functional groups, and framework topology on CO₂ adsorption [88]; (2) the reproduction of experimentally observed steps in the adsorption isotherm (as a function of pressure) due to CO₂ condensation (i.e. cluster formation) in the pores [99, 100]; (3) using the ideal adsorbed solution theory (IAST) to reveal non-trivial multi-component effects, including the effects of water vapor, in mixed-gas adsorption isotherms that can significantly affect CO₂ selectivity and separation [101]; (4) novel graphics processor unit (GPU) based simulations that has enabled the large-scale screening of hundreds of thousands of zeolite structures with optimal “parasitic” energy requirements for CO₂ capture [81]. There has also been some progress in simulating flexible frameworks and the effects of electronic polarization, although at a significantly higher computational cost. For more details on CO₂ capture simulations in molecular sieve materials (zeolites, MOFs, ZIFs) we refer the reader to some excellent reviews [102-105].

A second class of membrane materials amenable to modeling are the ones employing the solution-diffusion mechanism, which usually involves an active polymeric component deposited on an organic or inorganic substrate [106, 107]. Most separation strategies with polymer membranes employ the so-called asymmetric membrane configuration, which in its simplest form consist of a relatively dense, thin surface layer (skin) supported on an open, much thicker porous substrate. The skin layer is the active membrane and is designed with high values of selectivity toward the gas of interest, CO₂ in our case. Since high values of selectivity is almost always accompanied by low values of permeability, the skin layer needs to be thin in order to ensure good permeance (P/L), while the porous substrate provides mechanical support and an easy transport path for the separated gas downstream.

Polymeric membranes are typically dense and nonporous. Thus, for a gas to permeate through a polymer it first needs to get incorporated, i.e., dissolve in the matrix, followed by diffusive transport of the dissolved species. Thus, the permeability (P) of a gas through the membrane is a product of two terms: its solubility (S) and diffusivity (D), i.e., $P = D.S$. To compute D and S atomistically one would, in principle, like to use the following steps:

- Generation of amorphous polymer structure using a rotational isomeric state (RIS) theory [108]

- Solubility calculation using grand canonical Monte Carlo (GCMC) based sorption simulations [109] or an implicit-solvent quantum chemical model like COSMO-RS [28]
- Diffusivity calculations using classical molecular dynamics (MD) and/or Transition State Theory (TST) [110-112]

Although there are several multi-scale modeling and simulation examples of gas separation and transport in such materials (see [113] and references therein), including atomistic MD, MC, QM, QM/MM, QSPR/QSAR, CFD (computational fluid dynamics), and mesoscale DPD (dissipative particle dynamics) that can provide useful trends, there are several major challenges for the above modeling strategy to have the quantitative precision needed for the design of new separation membranes. These challenges include:

- For polymers and polymeric blends with complex functional groups and repeat patterns the real structures could be more complicated than generated by RIS, and do typically contain density variations, defects, voids, and a complex distribution of free volumes, all of which need to be accounted for to compute S and D accurately. Accounting for structural defects and density variations are even more important for nanostructured films, where the performance might show strong dependence on film thickness [114] (see Fig. 6);
- In a dense glassy polymer the Diffusivity D could be too slow for MD simulations. TST-based simulations require mapping out a topologically complex energy landscape;
- In case of rubbery polymers, gas diffusion could be strongly influenced by the slow structural relaxation of the polymer, which is difficult to model using molecular mechanics.

Given the above challenges, a correlation-based empirical approach appears more practical at this time [115]. One such approach, based on group contributions to free volume was developed in the late 1990s [116]. In this approach, the permeability P_i of a gas species i in a polymer is assumed to be given by the functional form $P_i = A_i \exp(-B_i / FFV_i)$, where A_i and B_i are gas-dependent constants, and FFV_i is the fractional free volume of the polymer, which is also assumed to depend on the penetrant gas as well. The quantity FFV_i is computed as a sum of group-contribution to van der Waals volume with coefficients depending both on the gas and the functional group. Another popular empirical approach is based on topological information about the polymer, more specifically

connectivity indices derived from graph theory, as implemented in the code SYNTHIA [117]. This approach does not depend on a database of functional group contributions, and thus can be applied to most new polymer formulations and designs. Such an approach can be used to predict many important polymer properties, including solubility and transport of gases, which can in turn be used study gas separation through membranes [118]. Robeson [119, 120] has analyzed the performance of a large number of polymers in terms of permeability and selectivity and created upper bound curves for different pairs of gases to be separated. A simple correlation between permeability and selectivity based on the kinetic diameters of the permeating gases has been used to rationalize such upper bound curves.

The above approach is intended for situations where the gas molecule physisorbs and diffuses as a chemically unreacted species. In facilitated transport membranes, where CO_2 typically dissolves and diffuses as HCO_3^- ions and then converts back to CO_2 in the downstream, one needs to use approaches similar to that described in sections 5.1 and 5.3.

6. Summary

The main purpose of this paper was to show that there are multiple possible strategies toward meeting the challenge of carbon capture while remaining viable in terms of speed, efficiency, and economics. The success of any given strategy depends on the capture materials used, the associated process engineering, and compatibility with the technology/industry from which CO_2 is intended to be captured from. Performance of any new materials comes down to the basic chemistry and interactions at the atomic level, and molecular modeling is a powerful tool that can help accelerate the process of discovery, design, or screening of materials for optimal performance. There are many situations, especially where deep chemical or molecular kinetic insights are needed, when one would like to embark on a truly atomistic first-principles approach, e.g., DFT-based QM simulations, or a classical MD or MC approach with well-validated interatomic potentials (force-fields) coupled with advanced simulation techniques. In principle, such approach would allow one to study any chemistry with CO_2 , or allow the computation of free energies, derived thermodynamic quantities, or important physicochemical properties of the capture medium. At the same time, there are also situations where a more pragmatic approach consists of using more approximate schemes that allow for faster semi-accurate results, so that one can perform reliable screening of a large number of possible candidates.

Such an approach, for instance, is already established in the field of drug discovery and now getting more and more popular in materials discovery as well. Several examples in this paper (section 5) illustrate this point, including: (1) the use of a COSMO-RS based implicit solvent scheme to: (i) compute the heats of CO₂ absorption in a primary and a tertiary amine, and (ii) to screen for an ionic liquid with high efficiency in CO₂ dissolution; (2) the development of a free-volume-based correlation and connectivity index to screen polymer membranes for high CO₂ permselectivity. Mention was also made of the development of molar volume-based correlations to estimate important thermo-physical properties of ILs, e.g., density, viscosity, specific heat, and melting point. Extensive work on equation-of-state or correlation-based methods to model vapor-liquid-equilibrium (VLE) and liquid-liquid equilibrium (LLE) using statistical associating fluid theory (SAFT) and related models should add useful knowledge and insights toward the discovery and optimization of novel liquid capture systems, e.g., advanced amines or task-specific ILs. Finally, regular periodic structures like zeolites, MOFs, and ZIFs are amenable to large-scale automated *in silico* screening for CO₂ capture efficiency, as has recently been demonstrated.

Acknowledgements:

The work at LLNL was performed under the auspices of the U.S. Department of Energy by Lawrence Livermore National Laboratory under Contract DE-AC52-07NA27344.

References

1. See Wikipedia article: http://en.wikipedia.org/wiki/Carbon_capture_and_storage.
2. J. David, H. Herzog, "The Cost of Carbon Capture," *Proceedings of the Fifth International Conference on Greenhouse Gas Control Technologies*, Cairns, Australia, **2000**, 985-990.
3. O. Işlegen, S. Reichelstein, *Management Science* **2011**, 57, 21.
4. G. T. Rochelle, *Science* **2009**, 325, 1652.
5. R. D. Deshmukh, A. E. Mather, *Chem. Eng. Sci.* **1981**, 36, 355.
6. F.-Y. Jou, A. E. Mather, F. D. Otto, *Can. J. Chem. Eng.* **1995**, 73, 140.
7. J. Gabrielsen et al., *Ind. Eng. Chem. Res.* **2005**, 44, 3348.
8. D. M. Austgen et al., *Ind. Eng. Chem. Res.* **1989**, 28, 1060.
9. Y. Liu, L. Zhang, S. Watanasiri, *Ind. Eng. Chem. Res.* **1999**, 38, 2080.
10. E. T. Hessen, T. Haug-Warberg, H. F. Svendsen, *Chem. Eng. Sci.* **2010**, 65, 3638.
11. W. Bottinger, M. Maiwald, H. Hasse, *Fluid Phase Equilibria* **2008**, 263, 131.
12. W. Bottinger, M. Maiwald, H. Hasse, *Ind. Eng. Chem. Res.* **2008**, 47, 7917.
13. M. K. Aroua, A. Benamor, M. Z. Haji-Sulaiman, *Ind. Eng. Chem. Res.* **1999**, 44, 887.
14. F.-Y. Jou, F. D. Otto, A. E. Mather, *Ind. Eng. Chem. Res.* **1994**, 33, 2002.
15. J. K. Carson, K. N. Marsh, A. E. Mather, *J. Chem. Thermodynamics* **2000**, 32, 1285.
16. N. McCann, M. Maeder, M. Attalla, *Ind. Eng. Chem. Res.* **2008**, 47, 2002.
17. C. Mathonat, V. Majer, A. E. Mather, J.-P. E. Grolier, *Fluid Phase Equilib.* **1997**, 140, 171.
18. I. Kim, H. F. Svendsen, *Ind. Eng. Chem. Res.* **2007**, 46, 5803.
19. F. Leder, *Chem. Eng. Sci.* **1971**, 26, 1381.
20. H. Hikita, S. Asai, H. Ishikawa, M. Honda, *Chem. Eng. J.* **1977**, 13, 7.
21. P. M. M. Blauwhoff, G. F. Versteeg, W. P. M. van Swaaij, *Chem. Eng. Sci.* **1983**, 38, 1411.
22. M. H. Jamroz, J. C. Dobrowoloski, M. A. Borowiak, *J. Mol. Struct.* **1997**, 404, 105.
23. E. F. da Silva, H. F. Svendsen, *Ind. Chem. Chem. Res.* **2006**, 45, 2497.

24. B. Arstad, R. Blom, O. Swang, *J. Phys. Chem. A* **2007**, *111*, 1222.
25. M. Ismael *et al.*, *Int. J. Greenh. Gas. Con.* **2009**, *3*, 612.
26. A. Klamt, G. Schüürmann, *J. Chem. Soc. Perkin. Trans.* **1993**, *2*, 799.
27. A. Klamt, *J. Phys. Chem.* **1995**, *99*, 2224.
28. A. Klamt, *COSMO-RS: From Quantum Chemistry to Fluid Phase Thermodynamics and Drug Design*, Elsevier, 2005. The commercial implementation, COSMOtherm, C2.1 Release 01.10 was used in this work.
29. H. Yamada *et al.*, *Ind. Eng. Chem. Res.* **2010**, *49*, 2449.
30. R. Ahlrichs, M. Bär, M. Häser, H. Horn, C. Kölmel, *Chem. Phys. Lett.* **1989**, *162*, 165.
31. A. Schäfer, A. Klamt, D. Sattel, J. C. W. Lohrenz, F. Eckert, *Phys. Chem. Chem. Phys.* **2000**, *2*, 2187.
32. A. D. Becke, *Phys. Rev. A* **1988**, *38*, 3098.
33. J. P. Perdew, *Phys. Rev. B* **1986**, *33*, 8822.
34. J. P. Perdew, *Phys. Rev. B* **1986**, *34*, 7406.
35. K. Eichkorn, F. Weigend, O. Treutler, R. Ahlrichs, *Theor. Chim. Acta* 1997, **97**, 119.
36. A. Schäfer, C. Huber, R. Ahlrichs, *J. Chem. Phys.* 1994, **100**, 5829.
37. P. Nagy, *J. Mol. Struct-Theochem* **1989**, *201*, 271.
38. H. A. Al-Ghawas, D. P. Hagewiesche, G. Ruiz-Ibanez, O. C. Sandall, *J. Chem. Eng. Data* **1989**, *34*, 385.
39. R. H. Weiland *et al.*, *Ind. Eng. Chem. Res.* **43** (1998) 378.
40. T. G. Amundsen, L. E. Øi, D. A. Eimer, *Ind. Eng. Chem. Res.* **54** (2009) 3096.
41. J. M. Bernal-garcia *et al.*, *J. Chem. Eng. Data* 48 (2003) 1442.
42. A. Maiti, W. L. Bourcier, R. D. Aines, *Chem. Phys. Lett.* **2011**, *509*, 25.
43. See <http://accelrys.com/products/materials-studio/> .
44. H. Sun, *J. Phys. Chem. B* **102** (1998) 7338.
45. H. C. Andersen, *J. Chem. Phys.* **72** (1980) 2384.
46. P. P. Ewald, *Ann. Phys.* **64** (1921) 253.
47. M. P. Tosi, *Solid State Physics* **16** (1964) 107.

48. S. Bishnoi, G. T. Rochelle, *AIChE J.* **2002**, *48*, 2788.
49. H. Dang, G. T. Rochelle, *Separ. Sci. Technol.* **2003**, *38*, 337.
50. L. Koziol et al., *Inorg. Chem.* **2012**, *51*, 6803.
51. R. D. Rogers, K. R. Seddon, S. Volkov (eds), *Green Industrial Applications of Ionic Liquids*, NATO Science Series, Kluwer, Dordrecht, **2002**.
52. T. Welton, *Chem. Rev.* **1999**, *99*, 2071.
53. J. D. Holbrey, K. R. Seddon, *Clean Products and Processes* **1999**, *1*, 223.
54. J. Dupont, R. F. de Souza, P. A. Suarez, *Z. Chem. Rev.* **2002**, *102*, 3667.
55. J. Ilconich, C. Myers, H. Pennline, D. Luebke, *J. Membrane Sci.* **2007**, *298*, 41.
56. L. A. Blanchard, D. Hancu, D.; E. J. Beckman, J. F. Brennecke, *Nature* **1999**, *399*, 28; L. A. Blanchard, J. F. Brennecke, *Ind. Eng. Chem. Res.* **2001**, *40*, 2550.
57. L. A. Blanchard, Z. Y. Gu, J. F. Brennecke, *J. Phys. Chem. B* **2001**, *105*, 2437.
58. S. N. V. K. Aki, B. R. Mellein, E. M. Saurer, J. F. Brennecke, *J. Phys. Chem. B* **2004**, *108*, 20355.
59. S. J. Zhang, X. L. Yuan, Y. H. Chen, X. P. Zhang, *J. Chem. Eng. Data* **2005**, *50*, 230.
60. M. J. Muldoon, S. N. V. K. Aki, J. L. Anderson, J. K. Dixon, J. F. Brennecke, *J. Phys. Chem. B* **2007**, *111*, 9001.
61. A. M. Schilderman, S. Raeissi, C. J. Peters, *Fluid Phase Equilibria* **2007**, *260*, 19.
62. J. Kumelan, A. P.-S. Kamps, D. Tuma, G. Maurer, *J. Chem. Eng. Data* **2006**, *51*, 1802.
63. J. Kumelan, A. P.-S. Kamps, D. Tuma, G. Maurer, *J. Chem. Thermodynamics* **2006**, *38*, 1396.
64. C. Cadena, J. L. Anthony, J. K. Shah, T. I. Morrow, J. F. Brennecke, E. J. Maginn, *J. Am. Chem. Soc.* **2004**, *126*, 5300.
65. J. Deschamps, M. F. C. Gomes, A. A. H. Padua, *ChemPhysChem* **2004**, *5*, 1049.
66. B. L. Bhargava, S. Balasubramanian, *Chem. Phys. Lett.* **2007**, *444*, 242.
67. W. Shi, E. J. Maginn, *J. Phys. Chem. B* **2008**, *112*, 2045.
68. A. Maiti et al., *Phys. Chem. Chem. Phys.* **2008**, *10*, 5050.

69. A. Klamt, F. Eckert, M. Hornig, M. E. Beck, T. Burger, *J. Comp. Chem.* **2001**, *23*, 275.
70. K. Z. Sumon, A. Henni, *Fluid Phase Equilibr.* **2011**, *310*, 39.
71. Y. S. Sistla, A. Khanna, *J. Chem. Eng. Data* **2011**, *56*, 4045.
72. M. Gonzalez-Miquel, J. Palomar, S. Omar, F. Rodriguez, *Ind. Eng. Chem. Res.* **2011**, *50*, 5739.
73. J. Palomar, M. Gonzalez-Miquel, A. Polo, F. Rodriguez, *Ind. Eng. Chem. Res.* **2011**, *50*, 3452.
74. Z. Lei, B. Chen, C. Li, *Chem. Eng. Sci.* **2007**, *62*, 3940.
75. P. Kolář, H. Nakata, J.-W. Shen, A. Tsuboi, H. Suzuki, M. Ue, *Fluid Phase Equilibr.* **2005**, *228*, 59.
76. G. Soave, *Chem. Eng. Sci.* **1972**, *27*, 1197.
77. D. P. Tassios, *Applied Chemical Engineering Thermodynamics*, Springer-Verlag, Berlin, Germany (1993).
78. A. Maiti, *ChemSusChem* **2009**, *2*, 628.
79. S. Mortazavi-Manesh, M. Satyro, R. A. Marriott, *Can. J. Chem. Eng.* **2013**, *91*, 783.
80. X. Zhang, Z. Liu, W. Wang, *AIChE J.* **2008**, *54*, 2717.
81. L.-C. Lin et al., *Nat. Mater.* **2012**, *11*, 633.
82. J. Kim, A. Maiti, L.-C. Lin, J. K. Stolaroff, B. Smit, R. D. Aines, *Nat. Comm.* **2013**, *4*, 1694.
83. J. M. Slattery, C. Daguinet, P. J. Dyson, T. J. S. Schubert, I. Krossing, *Angew. Chem. Int. Ed.* **2007**, *46*, 5384.
84. U. P. R. M. Preiss, J. M. Slattery, I. Krossing, *Ind. Eng. Chem. Res.* **2009**, *48*, 2290.
85. E. D. Bates, R. D. Mayton, I. Ntai, J. H. Davis, *J. Am. Chem. Soc.* **2002**, *124*, 926.
86. B. E. Gurkan, J. C. de la Fuente, E. M. Mindrup, L. E. Ficke, B. F. Goodrich, E. A. Price, W. F. Schneider, J. F. Brennecke, *J. Am. Chem. Soc.* **2010**, *132*, 2116.
87. B. E. Gurkan, B. F. Goodrich, E. M. Mindrup, L. E. Ficke, M. Masel, S. Seo, T. P. Senftle, H. Wu, M. F. Glaser, J. K. Shah, E. Maginn, J. F. Brennecke, W. F. Schneider, *J. Phys. Chem. Lett.* **2010**, *1*, 3494.
88. R. Babarao, J.W. Jiang, *Langmuir* **2008**, *24*, 6270.
89. R. Babarao, J.W. Jiang, *Energy Environ. Sci.* **2008**, *1*, 139.
90. R. Krishna, *J. Phys. Chem. C* **2009**, *113*, 19756.

91. R. Krishna, J. M. van Baten, *J. Membrane Sci.* **2010**, *360*, 323.
92. B. Liu, B. Smit, *Langmuir* **2009**, *25*, 5918.
93. Z. R. Herm et al., *J. Am. Chem. Soc.* **2011**, *133*, 5664.
94. J. H. Lan et al., *ACS Nano* **2010**, *4*, 4225.
95. Y.-S. Bae et al., *Langmuir* **2008**, *24*, 8592.
96. B. Liu, B. Smit, *J. Phys. Chem. C* **2010**, *114*, 8515.
97. A. O. Yazadin et al., *J. Am. Chem. Soc.* **2009**, *131*, 18198.
98. J. Kim et al., *J. Am. Chem. Soc.* **2012**, *134*, 18940.
99. K.S. Walton, A. R. Millward, D. Dubbeldam, H. Frost, J. J. Low, O. M. Yaghi, R. Q. Snurr, *J. Am. Chem. Soc.* **2008**, *130*, 406.
100. R. Krishna, J. M. van Baten, *Langmuir* **2010**, *26*, 3981.
101. A.O. Yazaydin, A.I. Benin, S.A. Faheem, P. Jakubczak, J. J. Low, R.R. Willis, R.Q. Snurr, *Chem. Mater.* **2009**, *21*, 1425.
102. D. M. D'Alessandro, B. Smit, J. R. Long, *Angew. Chem. Int. Ed.* **2010**, *49*, 6058.
103. B. Smit, T. L. M. Maesen, *Chem. Rev.* **2008**, *108*, 4125.
104. T. Duren, Y.-S. Bae, R. Q. Snurr, *Chem. Soc. Rev.* **2009**, *38*, 1237.
105. R. Krishna, *Chem. Soc. Rev.* **2012**, *41*, 3099.
106. C. E. Powell, G. G. Qiao, *J. Membrane Sci.* **2006**, *279*, 1.
107. C. A. Scholes, S. E. Kentish, G. W. Stevens, *Recent Pat. Chem. Eng.* **2008**, *1*, 52.
108. P. J. Flory, *Statistical Mechanics of Chain Molecules*, Wiley, New York (1969).
109. D. Frenkel and B. Smit, *Understanding Molecular Simulation – from Algorithms to Applications*, Academic Press, San Diego, 1996.
110. A. A. Gusev, S. Arizzi, U. W. Suter and D. J. Moll, *J. Chem. Phys.* **1993**, *99*, 2221.
111. A. A. Gusev, S. Arizzi and U. W. Suter, *J. Chem. Phys.* **1993**, *99*, 2228.
112. M. L. Greenfield, D. N. Theodorou, *Macromolecules* **1993**, *26*, 5461.

113. E. Tocci, P. Pullumbi, *Multi-scale Molecular Modeling Approaches for Designing/Selecting Polymers used for Developing Novel Membranes*, Book Chapter 1, in *Membrane Engineering for the Treatment of Gases*, eds. E. Drioli and G. Barbieri, RSC Publishing, 2011.
114. C. M. Spadaccini, E. V. Mukerjee, S. A. Letts, A. Maiti, and K. C. O'Brien, *Energy Procedia* **2011**, 4, 731.
115. V. A. Kusuma et al., *Structure/Property Characteristics of Polar Rubbery Membranes for Carbon Dioxide Removal*, Book Chapter 35, in *Advanced Membrane Technology and Applications*, eds. N. N. Li, A. G. Fane, W. S. Winston Ho, and T. Matsuura, John Wiley and Sons, 2008.
116. J. Y. Park, D. R. Paul, *J. Membr. Sci.* **1997**, 125, 23.
117. J. Bicerano, *Prediction of Polymer Properties*, third edition, Marcel Dekker, New York (2002).
118. R. Recio et al., *J. Membrane Sci.* **2007**, 293, 22.
119. L.M. Robeson, *J. Membr. Sci.* **1991**, 62, 165.
120. L. M. Robeson, *J. Membr. Sci.* **2008**, 320, 390.

Table 1: Computed heats of CO₂ absorption (ΔH) per mole of CO₂ at 25 °C in 30 wt% MEA and 45 wt% MDEA solutions. Reaction R1 involves the formation of carbamate ions, while R2 and R3 involve the formation of HCO₃⁻ ions. See text for more details.

Reaction	Amine/water ratio	CO ₂ loading	ΔH (kJ/mol)
R1	30 wt% MEA	0.0	-78.8
		0.25	-82.1
		0.5	-81.1
R2	30 wt% MEA	0.0	-60.6
		0.25	-63.0
		0.5	-64.8
		0.75	-66.3
		1.0	-67.6
R3	45 wt% MDEA	0.0	-47.2
		0.25	-46.6
		0.5	-45.6
		0.75	-44.4
		1.0	-42.8

Table 2. Chemical names, molecular weight, and class categories of the cations in Fig. 4.

Acronym	Chemical Name	Molecular Weight (g/mol)	Class
[emim]	1-ethyl-3-methyl-imidazolium	111.2	imidazolium
[bmim]	1-butyl-3-methyl-imidazolium	139.2	imidazolium
[hmim]	1-hexyl-3-methyl-imidazolium	167.3	imidazolium
[omim]	1-octyl-3-methyl-imidazolium	195.3	imidazolium
[tma]	tetra-methyl-ammonium	74.1	ammonium
[tea]	tetra-ethyl-ammonium	130.3	ammonium
[tba]	tetra-n-butyl-ammonium	242.5	ammonium
[tbp]	tetra-butyl-phosphonium	259.4	phosphonium
[ttp]	trihexyl-tetradecyl-phosphonium	483.9	phosphonium
[tmg]	tetra-methyl-guanidinium	116.2	guanidinium
[hmg]	hexa-methyl-guanidinium	144.2	guanidinium
[ppg]	n, n, n, n, n-pentamethyl-n-propyl-guanidinium	172.3	guanidinium

Table 3. Chemical names, molecular weight, and class categories of the anions in Fig. 5.

Acronym	Chemical Name	Molecular Weight (g/mol)
[BF ₄]	tetrafluoroborate	86.8
[PF ₆]	hexafluorophosphate	145.0
[Tf ₂ N]	bis(trifluoromethylsulfonyl)imide	280.1
[NO ₃]	nitrate	62.0
[TfO]	trifluoromethanesulfonate	149.1
[FEP]	tris(pentafluoroethyl)trifluorophosphate	445.0

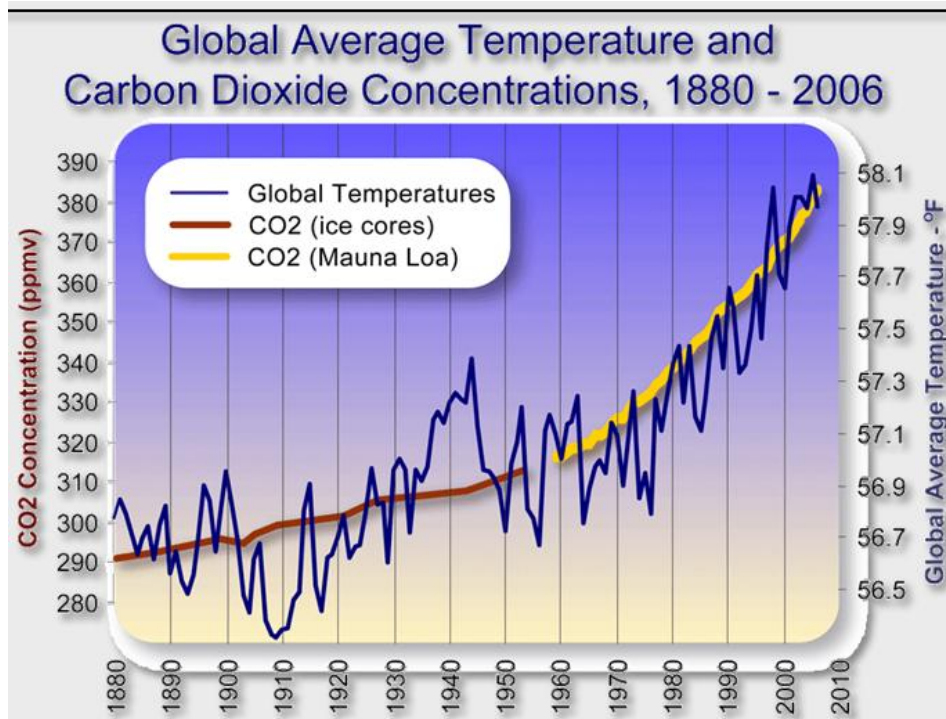


Fig 1. Historical data on the average CO₂ concentration in the atmosphere and the average world temperature since 1880. Courtesy: Michael Ernst, The Woods Hole Research Center.

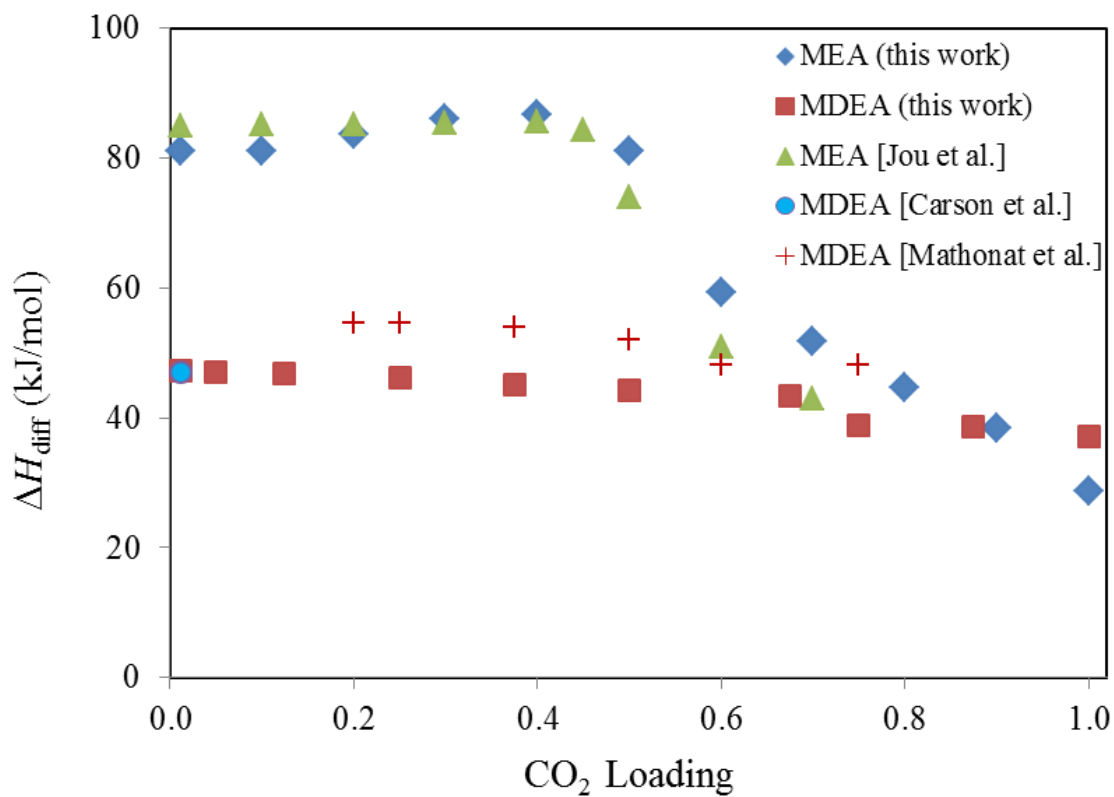


Fig 2. The differential heat of absorption (per mole of CO_2) in a 30 wt% MEA solution and 45 wt% MDEA solution as a function of CO_2 loading (mol CO_2 / mol amine) computed from the estimated heat of absorption of Table 1. Three sets of experimental data are also provided for comparison: Jou et al. [14], Carson et al. [15], and Mathonat et al. [17].

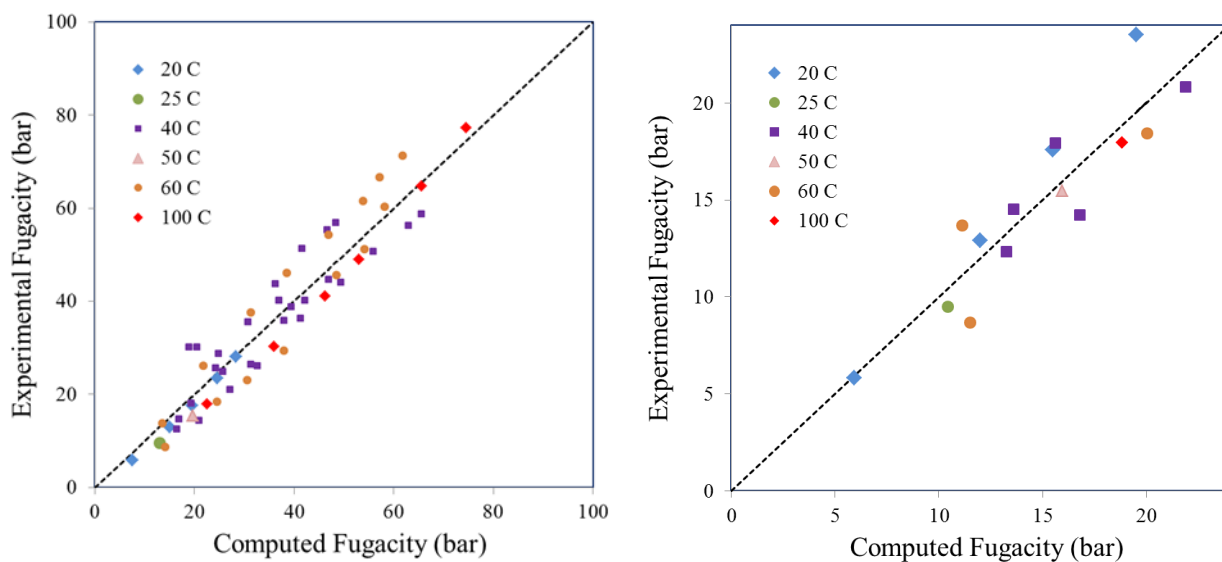


Fig 3. Computed versus experimental fugacity using the two-parameter model for $\mu_{ig}(T)$ (see text): (left) parameters with values $\mu_{ig}(T_c) = -4.10$ kcal/mol and $\alpha = -0.019$ kcal/mol/K optimized for the whole pressure range; (right) parameters with values $\mu_{ig}(T_c) = -3.97$ kcal/mol and $\alpha = -0.019$ kcal/mol/K optimized for the lower pressure region (~ 20 bar or lower) with the aim of estimating accurate Henry's constants. The experimental data are from references [56-63], and correspond to different temperatures varying between 20–100 °C (color coded).

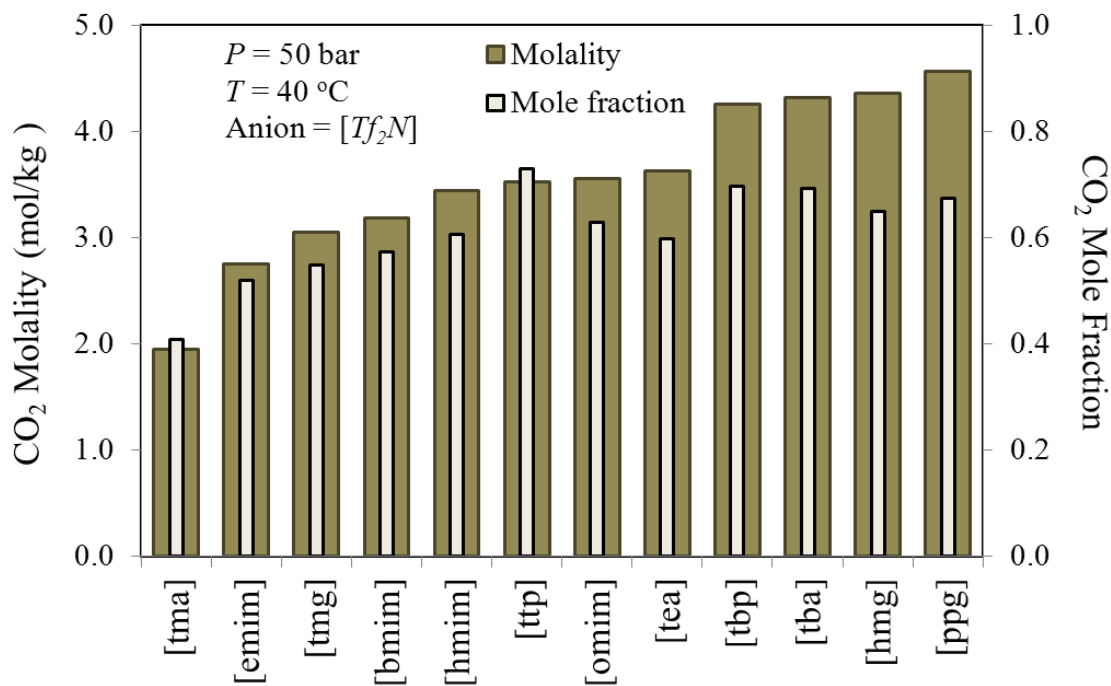


Fig. 4. Computed CO₂ solubility in various ILs as a function of cations for a fixed anion [Tf₂N] at T = 40 °C and P = 50 bar. The solubility is computed in two different scales: molality scale (mol CO₂/ kg solvent) and mole-fraction. Fully functionalized ammonium, phosphonium, and guanidinium cations appear to possess higher CO₂ solubility as compared to imidazolium, the most commonly studied class of cations in the experimental literature. In this group, the IL [ppg][Tf₂N] possesses the highest molal solubility, while the IL [ttp][Tf₂N] possesses the highest mole-fraction solubility of CO₂. The IL acronyms are explained Tables 2 and 3.

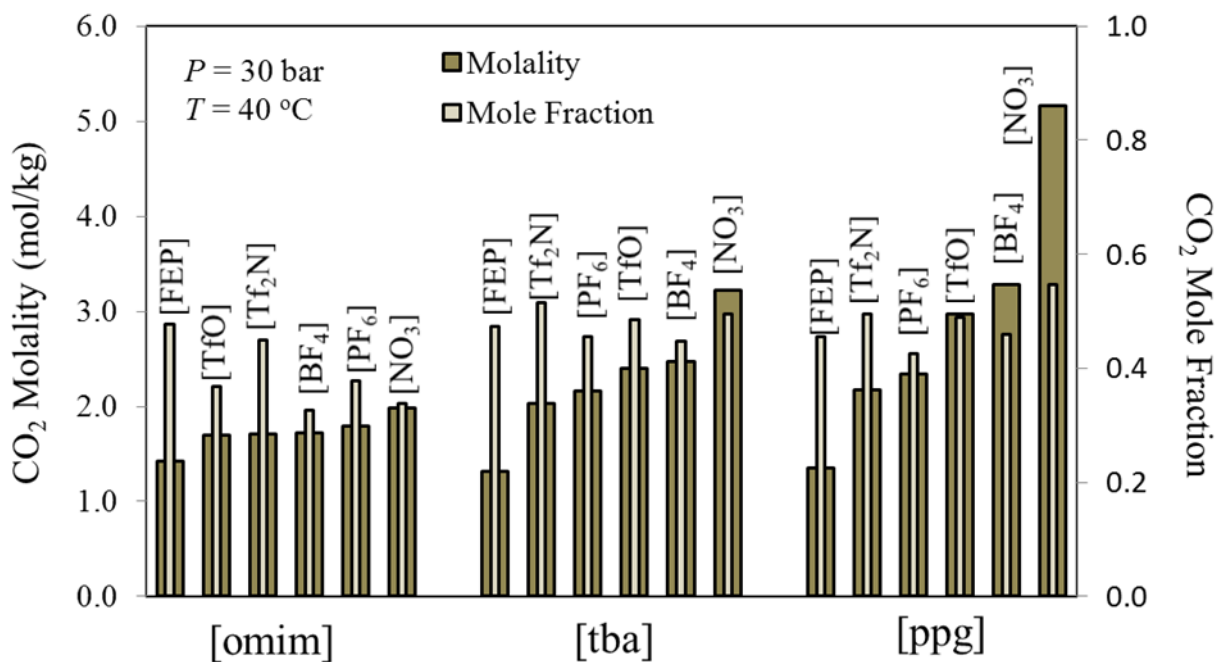


Fig. 5. Computed CO₂ solubility in various ILs as a function of six different anions and three different cations belonging to the imidazolium ([omim]), ammonium ([tba]), and guanidinium ([ppg]) classes; T = 40 °C and P = 30 bar. The solubility is computed in two different scales: molality scale (mol CO₂/ kg solvent) and mole-fraction.

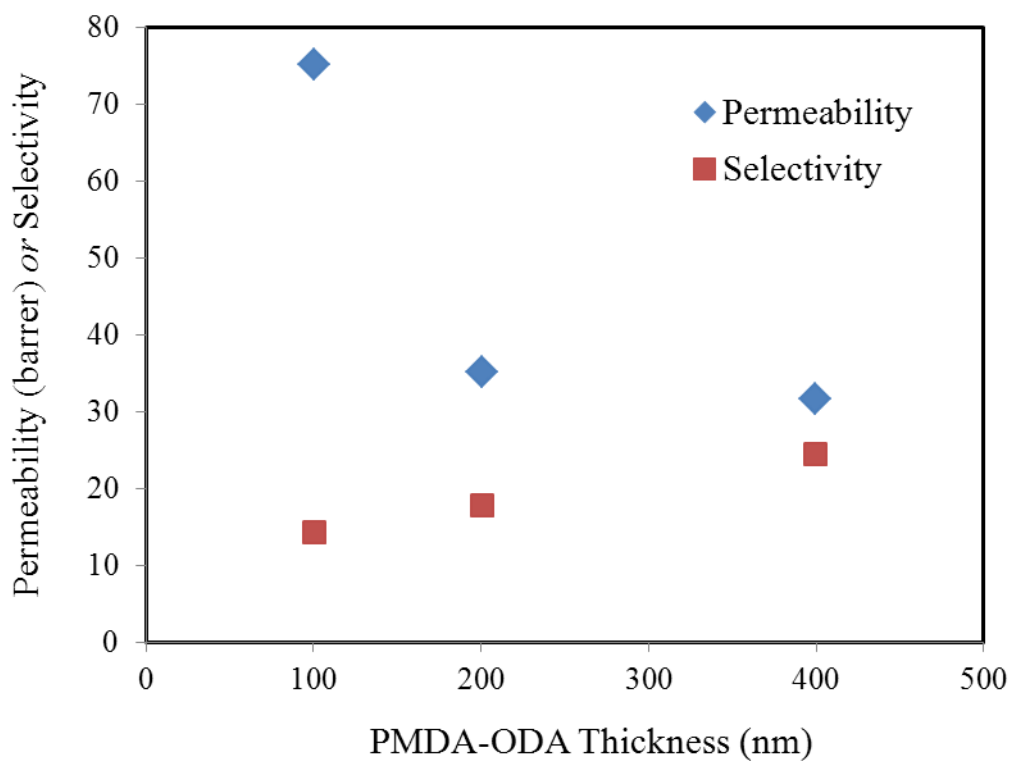
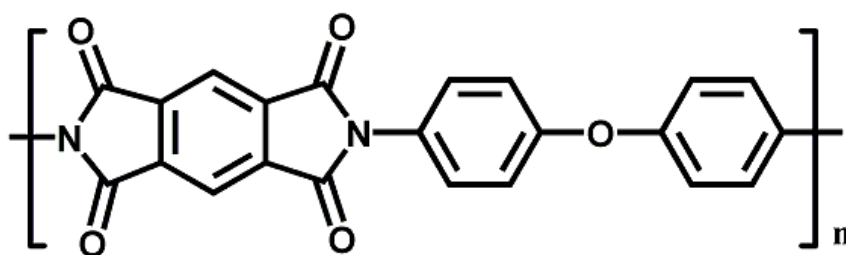


Fig 6. CO₂/N₂ selectivity and CO₂ permeability vs. thickness of the Pyromellitic dianhydride-oxydianiline (PMDA-ODA) membrane. A stick representation of the molecular structure of the monomer is shown on top. The PMDA-ODA membranes were created by a LLNL-developed solvent-less vapor deposition technique followed by an in-situ polymerization (SLIP) process. The above results are based on single-component gas permeation tests for films with thicknesses between 100-400 nm [114].